Pergamon

Geochimica et Cosmochimica Acta, Vol. 62, No. 5, pp. 867–882, 1998

0016-7037/98 $19.00 + .00

PII S0016-7037(98)00023-4

The effect of temperature on the partitioning of nickel, cobalt, manganese, chromium, and vanadium at 9 GPa and constraints on formation of the Earth's core

CHRISTINE K. GEßMANN* and DAVID C. RUBIE
Bayerisches Geoinstitut, Universität Bayreuth, D-95440 Bayreuth, Germany

(*Received June* 9, 1997; *accepted in revised form November* 11, 1997)

Abstract—The distribution of the elements Ni, Co, Mn, Cr, and V between liquid Fe-Ni-metal and magnesiowüstite solid solutions is investigated at 9 GPa in the temperature range 1800–2400°C. The variation of starting material enables the temperature effects to be determined at different redox conditions, although the buffering capacity of the sample plus high pressure assembly appears to be limited at temperatures above 2200°C. The observed metal-magnesiowüstite distribution coefficients (normalized to D_{Fe}) for the elements Ni and Co show a weak decrease with increasing temperature while those of Mn, Cr, and V progressively increase. The increasingly siderophile behaviour of Mn, Cr, and V with increasing temperature at high pressure is consistent with their depletion in the Earth's mantle being at least partly a consequence of core-mantle fractionation. The presence of silicate melt in some of the experiments also provides metal-silicate distribution coefficients as a function of temperature. The $K_DM^{met/sil}$ values for Mn, Cr, and V also increase with temperature. The metal-silicate distribution coefficients for Cr and V are slightly higher than those for metal-oxide partitioning while the results for Mn show larger differences. Manganese partitions preferentially into silicate phases, while Cr and V partition into magnesiowüstite. Comparison of the new metal-oxide partitioning data with previous results suggests that the magnesiowüstite composition has a strong influence on Ni partitioning. The distribution coefficients are extrapolated to higher temperatures in order to test the homogenous accretion model of core formation. Constraints on the solubility of Si and O in liquid metal are also obtained at 9 GPa and appear to preclude either of these elements as major light components in the Earth's core. *Copyright © 1998 Elsevier Science Ltd*

1. INTRODUCTION

The major differentiation event in the early history of the Earth was the formation of its iron-rich metallic core. A knowledge of the process of core formation is essential for the understanding of the overall processes involved in the formation of planets. One important constraint on the processes of core formation is the abundance of siderophile elements in the Earth's mantle. If core formation involved equilibrium processes between the segregating metal and mantle phases (i.e., silicate liquid in a magma ocean or mantle minerals under subsolidus conditions), the abundance of siderophile elements remaining in the mantle after core formation should be a function of their partitioning behaviour. Experiments on liquid metal and coexisting silicate melt (model materials for core and mantle, respectively) have been performed to determine element partitioning behaviour. Metal-silicate distribution coefficients obtained from experiments at atmospheric pressure are too high to explain the abundances of siderophile elements in the mantle (e.g., Hillgren, 1991; Holzheid et al., 1994). Therefore, it has been suggested that the Earth's core formed by more complicated processes such as inefficient core formation or heterogeneous, multistage accretion including a giant impactor event rather than by equilibrium processes (e.g., Benz et al., 1986; Stevenson, 1990, O'Neill, 1991). Alternatively, it has been proposed that metal-silicate distribution coefficients will decrease with increasing temperature (Murthy, 1991, 1992) or with increasing pressure (e.g., Keppler and Rubie, 1993), and, therefore, an equilibrium model of core formation might still be viable.

In the last two decades, the development of the multianvil high-pressure apparatus has opened new possibilities for investigating element partitioning at pressure and temperature conditions of the Earth's mantle. Experimental studies at high pressures and temperatures have been performed in the system liquid metal-silicate melt to provide further constraints on core formation processes (e.g., Walker et al., 1993; Hillgren et al., 1994, 1996; Ohtani et al., 1995,1997; Thibault and Walter, 1995; Walter and Thibault, 1996; Li and Agee, 1996; Righter et al., 1997). In particular, Li and Agee (1996), Ohtani et al. (1997), and Righter et al. (1997) have proposed models of core formation which explain the mantle abundances of siderophile elements by metal-silicate equilibrium at the base of a magma ocean that extended to mid-mantle depths. In addition, element partitioning studies have also been performed on systems including mantle minerals. Urakawa (1991) investigated the partitioning of Ni between metal and magnesiowüstite, while, for example, Kato et al. (1988a,b), Trønnes et al. (1992), Drake et al. (1993), McFarlane et al. (1994), and Agee et al. (1995) determined distribution coefficients between silicate minerals and silicate melts, and Kesson and Fitzgerald (1992) and Malavernge et al. (1997) reported siderophile element partitioning between magnesiowüstite and silicate perovskite.

* Author to whom correspondence should be addressed (christine.gessmann@uni-bayreuth.de).

The majority of these studies have concentrated on whether or not the influence of pressure is sufficient to solve the siderophile element anomaly. The effect of temperature on metal-silicate partitioning has been the subject of only a few studies (Walker et al., 1993; Hillgren et al., 1994; Thibault and Walter, 1995; Agee et al., 1995) in which changes in other variables (pressure, oxygen fugacity, and melt composition) may also have affected the results. For example, both Walker et al. (1993) and Hillgren et al. (1994) deduced the influence of temperature on element partitioning between metals and silicates by comparing their high-temperature, high-pressure results with experimental data obtained at lower temperatures and 1 bar (e.g., Jones and Drake, 1986; Drake et al., 1989). However, a distinct decrease in the metal-silicate and metal-oxide distribution coefficients with increasing pressure at constant temperature has been demonstrated for Ni and Co by Thibault and Walter (1995), Geßmann et al. (1995), and Li and Agee (1996). Consequently, the variations in partitioning behaviour reported in the studies of Walker et al. (1993) and Hillgren et al. (1994) cannot be attributed to temperature alone.

The results obtained in previous high-pressure partitioning studies indicate that careful and systematic investigations are required to decipher the influence of each individual variable (pressure, temperature, fO_2, composition, etc.). We have, therefore, performed a systematic experimental study of siderophile element partitioning (Fe, Ni, Co, Mn, Cr, and V) between liquid metal, magnesiowüstite, and (in some cases) silicate liquid as a function of temperature at constant pressure (9 GPa) and constrained fO_2 conditions. In addition to magnesiowüstite being an important lower-mantle phase, recent evidence suggests that it is an important liquidus phase at lower mantle conditions (Agee et al., 1995). The aim of the study is (1) to determine the effect of temperature on element partitioning in isolation from the effects of other variables, (2) to compare metal-oxide and metal-silicate distribution coefficients, and (3) to derive further constraints on the formation of the Earth's core.

2. EXPERIMENTAL

High pressure experiments have been performed using a 1200-tonne multianvil apparatus (Ito et al., 1984; Liebermann and Wang, 1992). The sample assembly consisted of an MgO (+5 wt% Cr_2O_3) octahedron with an edge length of 18 mm containing a $LaCrO_3$ heater with a stepped wall thickness to minimize thermal gradients (Canil, 1991; Rubie et al., 1993a). The octahedron was compressed using 32 mm tungsten carbide anvils (Toshiba grade F) with a truncation edge length of 11 mm using pyrophyllite gaskets. Temperature was monitored with an axial $W_3Re/W_{25}Re$ thermocouple (0.25 mm wire) with the thermocouple junction placed in direct contact with the end of an MgO capsule. The capsule had a wall thickness of 0.5 mm (mass ~18 mg) and contained ~6 mg of starting material. Pressure was calibrated using Bi phase transitions at room temperature and SiO_2 and Fe_2SiO_4 phase transformations at 1000 °C and 1450 °C (see Rubie et al., 1993b). The uncertainties in pressure and temperature are estimated to be ±0.5 GPa and ±40°C, respectively.

Starting materials were Fe-Ni powders doped with 1–1.5 wt% of various elements (Co, Mn, Cr, V, Ti) and varying amounts of Si which were added as elements or oxides (Table 1). The experiments have been performed with three different starting materials (i.e., 1a, 4a and 6a). While all the starting materials have similar Fe/Ni ratios and similar concentrations of the added trace elements, their Si and O contents vary (see Si/O ratios listed in Table 1). This variation results in different redox levels and the production of varying proportions of silicate melt.

Table 1. Composition of the starting materials.

#	Mix 1, 1a (1) (wt%)	Mix 4, 4a (1) (wt%)	Mix 6a (wt%)
Fe	72.59	59.50	61.12
Fe_3O_4			12.41
Ni	15.78	13.05	15.18
Co (1)	1.49 (1)	1.47 (1)	1.50
Mn	1.57	1.64	1.58
Cr	1.57	1.59	1.58
V		1.58	
V_2O_5	2.76		2.37
Si		1.78	
SiO_2	2.17	16.99	2.19
TiO_2	2.07	2.40	2.07
Fe/Ni	4.59	4.56	4.62
Si/O	0.317	0.971	0.158

Note: (1) Mix 1 and 4 without Co, Mix 1a and 4a with Co, respectively.

In each experiment, the sample was first pressurized to the desired pressure (9 GPa); the temperature was then raised at ~100°C /min to the desired run temperature (1800–2400 °C) and then held there for 5–20 min (Table 2). The sample was quenched by switching off the power to the $LaCrO_3$ furnace (initial quench rate ~400 °C/sec) and then decompressed over a period of 10–12 h. After completion of the experiment, the entire sample assembly was mounted in epoxy, and a section through the center of the sample was polished for electron microprobe analysis. Samples were analysed using a CAMECA SX50 electron microprobe (20 keV, 50 nA, 100 sec counting time for trace elements and 50 sec counting time for major elements). Fe metal, Ni metal, Co metal, forsterite, periclase, Cr_2O_3, $MnTiO_3$, and V_2O_5 were employed as standards. Although detection limits of around 50 ppm for the analysed elements under similar analysing conditions have been reported (Ramsden and French, 1990), the detection limits calculated employing the formula given by Brümmer (1977) based on the calibration data and analysing conditions are as follows: Mg - 110 ppm, Si - 100 ppm, Ti - 90 ppm, Fe - 250 ppm, Ni - 350 ppm, Co - 200 ppm, Mn – 120 ppm, Cr - 170 ppm, and V - 190 ppm. Oxygen contents in magnesiowüstite, silicate melt, and exsolved blobs in the quenched metal were calculated from element analyses and assumed stoichiometry (assuming divalent Mg, Fe, Ni, Co, and Mn, trivalent V and Cr, and a valence of 4+ for Si and Ti).

3. RESULTS

At the P-T conditions of the experiments, the Fe-Ni metal was in all cases a liquid and Fe, as well as other siderophile elements, diffused into the MgO capsule forming magnesiowüstite solid solutions. A backscattered electron image of a typical sample (Fig. 1a) shows the quenched liquid metal enclosed by the magnesiowüstite capsule wall. A distinctive feature of these experiments is the exsolution of spherical blobs within the metal liquid during the quench (Fig. 1b). Similar blobs were described by Ohtani and Ringwood (1984), Ito et al. (1995), and O'Neill et al. (1998). The latter authors have provided a detailed description and discussion of their origin. The blobs are distributed throughout the quenched metal sample except in a 50–100 μm wide zone adjacent to the metal-magnesiowüstite interface where they are absent (Fig. 1b).

Table 2. Experimental conditions, proportions of exsolved blobs in quenched metal, and observed phases in the run products. All experiments have been performed at 9 GPa.

Experiment #	Temperature [°C]	time [min]	Starting material Mix #	calculated oxygen fugacity [1]	Volume% blobs	Run products
1385	2200[2]	2	6a	- 1.51	5.90	Mw, Met
1371	2200	4	6a	- 1.45	5.98	Mw, Met
1383	2200	8	6a	- 1.53	5.81	Mw, Met
1352	2200	16	6a	- 1.50	5.77	Mw, Met
1245	1800	16	4	- 2.67	0.15	Mw, Met, Ol
1418	1900	16	4a	- 3.35	0.33	Mw, Met, Ol
1358	2000	16	4a	- 2.70	0.50	Mw, Met, Melt
1457	2100	10	4a	- 2.69	0.40	Mw, Met, Melt
1200	2200	16	4	- 2.71	0.32	Mw, Met, Melt
1547	2300	9	4a	- 2.29	1.44	Mw, Met, Melt
1312	2400	12	4a	- 1.95	3.28	Mw, Met, Melt
1554[3]	1800[2]	20	1a	- 1.94	0.00	Mw, Met
1549	1900	14	1	- 1.86	0.81	Mw, Met, Melt
1558	2000	16	1a	- 2.10	0.64	Mw, Met
1186	2200	16	1	- 2.07	1.95	Mw, Met, Melt
1551	2400	10	1a	- 1.74	4.28	Mw, Met

Note : Mw = magnesiowüstite, Met = quenched liquid metal, Ol = olivine, Melt = silicate melt

[1] oxygen fugacity calculated based on the Fe-FeO equilibrium; for details see text;

[2] temperature estimate based on power-temperature calibration with uncertainty of ±80°C;

[3] Temperature-reversal experiment;

They consist mainly of Si, Mn, O, Cr, Fe, and V and are chemically distinctly different from the surrounding metal (hereafter referred to as the metal matrix). Their composition is variable, and they consist predominantly of silicates or, in some cases, oxides, depending on temperature and fO_2 (for details see below). The blobs are interpreted to have formed by exsolution from a metal liquid which is homogeneous at the P-T conditions of the experiments. An enrichment of blob-forming elements has also been detected adjacent to the metal-capsule interface (for detailed discussion see below) and has been interpreted to form there by heterogeneous nucleation (O'Neill et al., 1998). Migration of this material through the liquid metal during the quench results in the 50–100 μm wide blob-free zone (Fig. 1b). In contrast, within the center of the liquid metal, blob formation is controlled by the kinetics of homogeneous nucleation. This interpretation is supported by a slow quench experiment (see O'Neill et al., 1998) in which blobs were absent even in the center of the quenched metal whereas the enrichment of several elements at the capsule-metal interface was still observed. A recalculation of the metal composition based on the volume fraction and the densities of the metal matrix and blobs is, therefore, required to determine distribution coefficients.

The volume fraction of blobs was determined from reflected-light optical micrographs using image analysis. The samples (avoiding the 50–100 μm wide marginal zones) were imaged at two different magnifications (50x and 100x) which gave fields of view of 100 μm × 100 μm and 50 μm × 50 μm, respectively. Between 30 and 130 such images (depending on magnification and sample size) were systematically measured and averaged for each sample. Most samples have been measured several times with varying magnifications, and the corresponding results generally agree within 10%. Where only one set of measurements was obtained, the error was, therefore, assumed to be ±10%. The measured area fraction of the blobs is proportional to their volume fraction because the analyzed area is representative for the whole sample (Underwood, 1970). In addition the

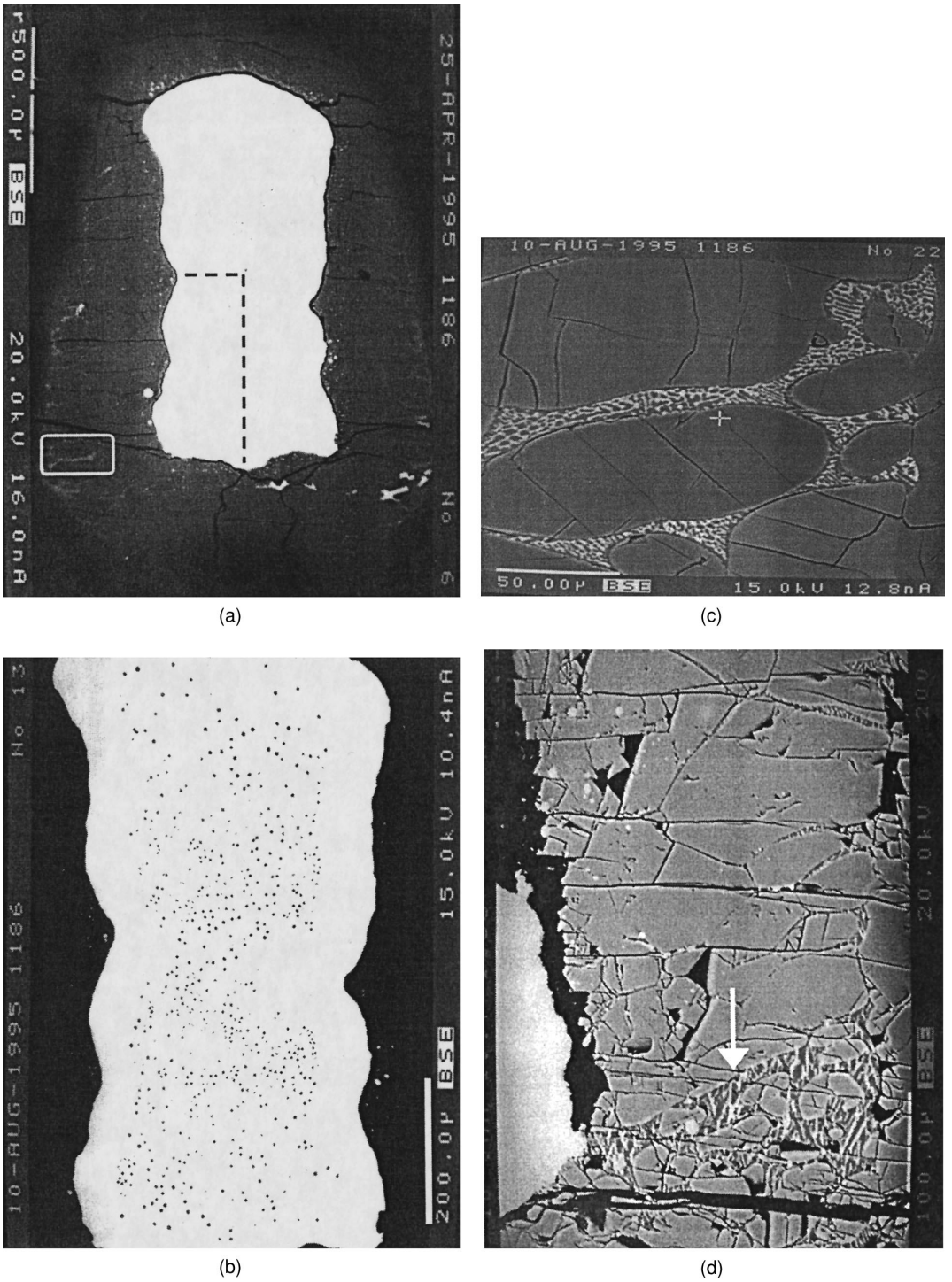

Fig. 1. (a) Backscattered electron image of sample 1186 showing the quenched liquid metal (white) surrounded by the magnesiowüstite capsule (grey). Small amounts of quenched silicate melt (light grey) are present in narrow veins within the magnesiowüstite; details of these veins can be seen in Fig. 1c which is an enlargement of the region enclosed by the white frame. Black cracks in the capsule walls formed during decompression. The dashed lines indicate the positions of the line profiles along which the homogeneity of the metal composition was checked routinely in all samples. Scale bar is 500 μm. (b) A higher magnification of the same sample showing small exsolved blobs in the quenched liquid metal. Note that the marginal region of the metal is free of these blobs. Scale bar is 200 μm. (c) A high magnification view of the region enclosed by the white frame in Fig. 1a showing small veins of silicate melt with typical quench structures which have formed predominantly along grain boundaries in the magnesiowüstite. Scale bar is 50 μm. (d) A close up view of the quenched liquid metal (lower left) and magnesiowüstite (grey) in sample 1558 showing a large pool of silicate melt with typical quench structures (indicated by arrow) which formed in contact with both phases. Scale bar is 100 μm.

blobs are approximately spherical and the microstructure is not usually anisotropic. The results, i.e., the volume fractions of the blobs, are listed in Table 2 for each experiment.

Silicon has been added to the starting material in order to vary the redox conditions. Besides this, either silicate liquid ($T \geq 2000°C$) or crystalline olivine ($T < 2000°C$) (compositions listed in Table 3) formed during the experiments by reaction with the capsule material. The silicate liquid occurs in varying amounts (depending on the Si and O contents of the starting material, i.e., Table 1) and is usually distributed along grain boundaries in the capsule wall in the form of veins 10–25 μm wide. Larger silicate melt pools frequently occur at grain boundary triple junctions. The silicate melt tends to migrate away from the liquid metal and sometimes becomes concentrated in the outer regions of the MgO capsule (Fig. 1a,c). In experiments in which a relatively large amount of silicate liquid is present, the melt forms broad veins and pools (Fig. 1d). Figure 1c,d show typical quench textures, which consist of interlocked Ti-poor and Ti-rich dendrites.

The chemical homogeneity of the metal matrix and of the magnesiowüstite was checked by analysing along line profiles. In the case of the quenched metal liquid, two orthogonal profiles were analysed for each sample (e.g., Fig. 1a). Analyses of the capsule material were made along two to five line profiles for each sample starting at the metal-oxide contact (hereafter referred to as the interface) and perpendicular to this interface. The step interval of the profiles was usually 10–15 μm, and the length of these line scans varied between 100 and 300 μm. The element concentrations along the measured profiles show generally homogeneous metal and magnesiowüstite compositions. As an example, line profiles for sample #1457 (2100°C, 10 min) are shown in Fig. 2 and indicate only slight compositional variations in both phases up to 200 μm from the interface. Fluctuations in Si and Cr contents, occasionally observed in the metal, appear to be coupled (Fig. 2b) and may be caused by blobs situated just below the polished surface of the sample. All elements show compositional profiles in the magnesiowüstite capsule wall which are generally flat up to several hundred microns from the interface (Fig. 2c,d). These profiles together with additional analyses indicate the composition of the entire capsule homogenized during the experiments. In the case of Fe, a compositional gradient is superimposed on the flat profile within 40–50 μm of the interface (Fig. 2d), as also shown schematically in Fig. 2e. A similar result is seen for V, although there is evidence that the profile which developed >50 μm from the interface was not completely flat (Fig. 2d). The localized compositional gradients close to the interface are believed to be diffusion profiles which developed during the quench. According to this interpretation, the composition of the capsule largely equilibrates with the liquid metal during the experiments, as a result of the rapid diffusion of cations over several 100 μm. During the quench, the capsule becomes chemically modified within ~40μm of the interface (see Fig. 2e). Based on this interpretation, distribution coefficients are calculated using magnesiowüstite compositions obtained at least 40 μm from the interface (see below).

Exceptions to the broad homogenous element concentration profiles in magnesiowüstite described above were observed in two low-temperature experiments at 1800° and 1900°C (# 1245 and # 1418) in which a Si-rich starting material was used (mix 4a). Instead of silicate liquid, a broad zone of olivine (50–200 μm wide) formed between the liquid metal and the magnesiowüstite. In these cases, the concentration profiles in magnesiowüstite are very short (e.g., 50 μm). In these experiments, magnesiowüstite compositions in equilibrium with the liquid metal were estimated from analyses obtained from close to the interface with olivine but with a relatively large uncertainty due to the compositional variations.

The enrichment of blob-forming elements at the interface, mentioned above and described by O'Neill et al. (1998), is usually not detected in these line profiles because of the relatively large spacing between individual analyses (Fig. 2). However, such enrichment was determined in some line profiles when the spacing between analyses was small (2–5 μm). Unlike O'Neill et al. (1998) we detected such element enrichment close to the interface only in some experiments. The absence of such enrichment in some of the run products can be correlated with a relatively small proportion of blobs in these experiments. In these cases, the concentration of blob-forming components adjacent to the interface is probably below the spatial and/or compositional detection limits of the electron microprobe.

The metal-oxide distribution coefficients $D_M^{met/ox}$ (= wt % element M in the metal/ wt % element M in the oxide) were obtained from analyses of element M in the quenched metal liquid (integrated blob and matrix compositions) and in the magnesiowüstite (normally obtained within a distance of 40–80 μm of the metal-oxide interface, cf. Fig. 2). Ten to thirty-five analyses of each phase (magnesiowüstite and metal matrix) and five to fifteen blob analyses were averaged, and the metal composition was calculated by integrating the metal matrix and the blob compositions based on their respective volume fractions and the estimated densities of the two phases (i.e., 8 g/cm^3 for the metal matrix, 4.5 g/cm^3 for the silicate-rich blobs and 5.7 g/cm^3 for the oxide-rich blobs). The distribution coefficients $D_M^{met/ox}$ were then calculated employing the respective mean values. Uncertainties in the distribution coefficients were derived by error propagation (Tables 3 and 4). The quoted errors are maximum values because the interdependencies of the components have been neglected when performing the error propagation.

Due to the generally small fraction of silicate melt present, the small dimensions of the veins and the quench textures, the silicate melt analyses have large uncertainties. Where possible, analyses have been obtained using a defocused electron beam (15–20 μm in diameter). In the case of narrow veins, a focused beam has been used to avoid contamination by the surrounding material and the average taken of a number of analyses. There were no significant differences between analyses obtained using focused and defocused beams on the same sample. Because of the larger

Table 3. Magnesiowüstite, metal, blob, and silciate compositions (in wt%) determined by electron microprobe analysis and calculated distribution coefficients $D_m^{met/ox}$ and $D_M^{met/sil}$ of experiments performed with the Si-rich starting material (mix 4, 4a).

# 1245 (1800°C)	magnesiowüstite	metal - matrix	blob	integr. metal	silicate	$D^{met/ox}$	$D^{met/sil}$
Mg	45,665 (1,011)	0,003 (0,003)	0,003 (0,001)	0,003 (0,003)	32,282 (0,759)		
Fe	4,863 (0,445)	82,375 (0,503)	22,646 (2,561)	82,327 (0,505)	1,873 (0,311)	16,93 (1,56)	43,97 (7,3)
Ni	0,040 (0,006)	17,823 (0,367)	4,001 (0,869)	17,812 (0,368)	0,035 (0,019)		
Ti	3,229 (0,275)	0,001 (0,001)	0,930 (0,028)	0,002 (0,001)	0,198 (0,089)		
Si	0,389 (0,079)	1,003 (0,075)	16,343 (0,854)	1,015 (0,075)	19,514 (0,283)	2,61 (0,56)	0,05 (0,004)
Mn	2,296 (0,100)	0,332 (0,016)	16,431 (1,157)	0,345 (0,017)	1,635 (0,238)	0,15 (0,01)	0,21 (0,03)
Cr	2,962 (0,368)	1,355 (0,030)	3,295 (0,162)	1,357 (0,030)	0,498 (0,110)	0,46 (0,06)	2,73 (0,61)
V	4,203 (0,445)	0,636 (0,053)	5,284 (0,527)	0,640 (0,053)	0,731 (0,203)	0,15 (0,02)	0,88 (0,25)
O	39,392 (0,211)		37,276 (0,928)	0,030 (0,001)	45,434 (0,368)		

# 1418 (1900°C)	magnesiowüstite	metal - matrix	blob	integr. metal	silicate	$D^{met/ox}$	$D^{met/sil}$
Mg	52,502 (0,487)	0,004 (0,003)	0,017 (0,002)	0,004 (0,003)	32,534 (0,497)		
Fe	2,214 (0,197)	82,764 (0,279)	6,673 (1,707)	82,619 (0,282)	1,072 (0,100)	37,36 (3,09)	77,06 (7,2)
Ni	0,026 (0,005)	13,309 (0,186)	0,386 (0,211)	13,285 (0,186)	0,030 (0,010)		
Co	0,011 (0,004)	2,358 (0,012)	0,117 (0,039)	2,354 (0,012)	0,008 (0,005)		
Ti	0,975 (0,083)	0,001 (0,001)	0,843 (0,053)	0,003 (0,001)	0,063 (0,010)		
Si	0,101 (0,016)	0,500 (0,034)	18,682 (0,440)	0,535 (0,035)	19,387 (0,199)	5,295 (0,77)	0,03 (0,002)
Mn	1,160 (0,090)	0,475 (0,024)	25,263 (0,702)	0,522 (0,026)	0,886 (0,108)	0,45 (0,04)	0,59 (0,07)
Cr	1,439 (0,113)	1,857 (0,097)	4,838 (0,095)	1,862 (0,097)	0,326 (0,050)	1,29 (0,12)	5,71 (0,92)
V	2,830 (0,318)	1,026 (0,110)	7,134 (0,422)	1,037 (0,111)	0,517 (0,084)	0,37 (0,05)	2,01 (0,39)
O	39,185 (0,369)		36,860 (0,191)	0,070 (0,001)	44,671 (0,407)		

# 1358 (2000°C)	magnesiowüstite	metal - matrix	blob	integr. metal	silicate - melt	$D^{met/ox}$	$D^{met/sil}$
Mg	49,571 (0,632)	0,007 (0,004)	0,026 (0,004)	0,007 (0,004)	32,108 (0,232)		
Fe	4,654 (0,331)	84,147 (0,162)	5,035 (0,126)	83,925 (0,162)	1,450 (0,080)	18,03 (1,29)	57,90 (3,2)
Ni	0,066 (0,011)	15,375 (0,164)	0,119 (0,020)	15,333 (0,163)	0,036 (0,018)	230,91 (38,44)	
Co	0,034 (0,001)	2,860 (0,013)	0,052 (0,010)	2,852 (0,013)	0,014 (0,004)	83,40 (2,12)	
Ti	0,655 (0,070)	0,001 (0,002)	0,387 (0,055)	0,002 (0,002)	0,064 (0,042)		
Si	0,115 (0,016)	0,390 (0,024)	18,829 (0,173)	0,442 (0,024)	19,353 (0,055)	3,85 (0,51)	0,02 (0,001)
Mn	1,499 (0,030)	0,365 (0,012)	23,436 (0,088)	0,430 (0,012)	0,853 (0,101)	0,29 (0,01)	0,50 (0,05)
Cr	1,878 (0,146)	1,304 (0,022)	5,623 (0,064)	1,316 (0,022)	0,298 (0,034)	0,70 (0,06)	4,41 (0,51)
V	3,539 (0,334)	0,555 (0,018)	8,963 (0,241)	0,578 (0,019)	0,406 (0,089)	0,16 (0,016)	1,42 (0,3)
O	38,633 (0,042)		39,676 (0,262)	0,111 (0,001)	44,355 (0,100)		

# 1457 (2100 °C)	magnesiowüstite	metal - matrix	blob	integr. metal	silicate - melt	$D^{met/ox}$	$D^{met/sil}$
Mg	53,433 (0,337)	0,022 (0,009)	0,074 (0,002)	0,022 (0,009)	30,460 (2,206)		
Fe	4,424 (0,121)	79,325 (0,358)	7,757 (2,634)	79,160 (0,363)	2,503 (0,732)	17,90 (0,50)	31,63 (9,33)
Ni	0,104 (0,016)	19,152 (0,757)	0,803 (0,521)	19,110 (0,757)	0,037 (0,013)	183,49 (29,11)	
Co	0,028 (0,003)	2,104 (0,017)	0,101 (0,049)	2,099 (0,017)	0,008 (0,004)	74,19 (7,82)	
Ti	0,537 (0,019)	0,001 (0,002)	0,846 (0,091)	0,003 (0,002)	1,763 (1,558)		
Si	0,051 (0,009)	0,640 (0,060)	22,448 (0,613)	0,691 (0,062)	18,925 (0,809)	13,50 (2,48)	0,04 (0,004)
Mn	1,093 (0,015)	0,335 (0,019)	23,381 (0,834)	0,388 (0,021)	1,453 (0,488)	0,36 (0,02)	0,27 (0,08)
Cr	1,366 (0,032)	1,049 (0,031)	4,205 (0,141)	1,056 (0,031)	0,631 (0,247)	0,77 (0,03)	1,67 (0,64)
V	1,334 (0,066)	0,225 (0,018)	2,372 (0,071)	0,230 (0,018)	0,537 (0,235)	0,17 (0,016)	0,43 (0,18)
O	38,461 (0,208)		38,524 (0,309)	0,089 (0,001)	44,481 (0,488)		

Table 3. (Continued).

# 1200 (2200°C)	magnesiowüstite	metal - matrix	blob	integr. metal	silicate - melt	$D^{met/ox}$	$D^{met/sil}$
Mg	53,503 (0,294)	0,002 (0,002)	0,086 (0,011)	0,002 (0,002)	31,278 (1,171)		
Fe	4,611 (0,125)	82,547 (0,400)	2,986 (0,258)	82,404 (0,399)	2,532 (0,655)	17,87 (0,49)	32,55 (8,44)
Ni	0,095 (0,010)	20,389 (0,274)	0,147 (0,026)	20,352 (0,273)	0,040 (0,017)	214,24 (23,49)	
Ti	0,515 (0,012)	0,001 (0,002)	0,779 (0,226)	0,003 (0,002)	1,336 (0,759)		
Si	0,035 (0,002)	0,821 (0,052)	24,306 (0,923)	0,864 (0,053)	18,991 (0,415)	25,03 (1,86)	0,045 (0,003)
Mn	0,949 (0,010)	0,333 (0,018)	24,894 (0,539)	0,377 (0,019)	1,368 (0,337)	0,40 (0,02)	0,28 (0,06)
Cr	1,102 (0,015)	1,051 (0,018)	3,104 (0,081)	1,055 (0,018)	0,467 (0,130)	0,96 (0,02)	2,26 (0,63)
V	1,603 (0,043)	0,389 (0,015)	2,440 (0,080)	0,393 (0,015)	0,578 (0,185)	0,25 (0,01)	0,68 (0,22)
O	38,983 (0,170)		38,996 (0,873)	0,070 (0,002)	44,915 (0,550)		

# 1547 (2300°C)	magnesiowüstite	metal - matrix	blob	integr. metal	silicate - melt	$D^{met/ox}$	$D^{met/sil}$
Mg	52,469 (0,320)	0,006 (0,003)	0,011 (0,004)	0,006 (0,003)	31,186 (0,931)		
Fe	7,354 (0,278)	79,616 (0,369)	17,088 (0,232)	78,922 (0,367)	3,800 (0,453)	10,73 (0,41)	20,77 (2,48)
Ni	0,165 (0,009)	21,656 (0,343)	0,161 (0,043)	21,417 (0,340)	0,052 (0,015)	129,93 (7,70)	410,74 (115,8)
Co	0,050 (0,002)	2,251 (0,012)	0,051 (0,007)	2,226 (0,012)	0,015 (0,004)	44,38 (1,69)	
Ti	0,292 (0,016)	0,002 (0,005)	0,009 (0,004)	0,003 (0,005)	0,991 (0,865)		
Si	0,045 (0,002)	0,038 (0,004)	15,367 (1,797)	0,208 (0,024)	18,381 (0,604)	4,67 (0,56)	0,01 (0,001)
Mn	0,647 (0,035)	0,054 (0,009)	14,180 (1,093)	0,211 (0,021)	0,721 (0,113)	0,33 (0,04)	0,29 (0,055)
Cr	0,921 (0,018)	0,426 (0,010)	9,787 (2,150)	0,530 (0,034)	0,266 (0,033)	0,58 (0,04)	2,00 (0,28)
V	0,824 (0,059)	0,053 (0,008)	7,325 (1,814)	0,134 (0,028)	0,250 (0,074)	0,16 (0,036)	0,54 (0,20)
O	37,942 (0,188)		34,573 (0,578)	0,384 (0,006)	43,682 (0,666)		

# 1312 (2400°C)	magnesiowüstite	metal - matrix	blob	integr. metal	silicate - melt	$D^{met/ox}$	$D^{met/sil}$
Mg	49,311 (0,456)	0,002 (0,002)	0,270 (0,163)	0,010 (0,007)	27,962 (0,695)		
Fe	10,738 (0,511)	80,157 (0,292)	57,943 (1,558)	79,490 (0,330)	9,199 (0,763)	7,40 (0,35)	8,64 (0,72)
Ni	0,240 (0,010)	21,083 (0,412)	1,017 (0,680)	20,481 (0,420)	0,095 (0,023)	85,38 (3,86)	214,83 (52,4)
Co	0,118 (0,007)	3,811 (0,040)	0,403 (0,257)	3,709 (0,047)	0,053 (0,008)	31,37 (1,88)	69,55 (10,58)
Ti	0,214 (0,004)	0,001 (0,001)	0,055 (0,053)	0,002 (0,003)	0,356 (0,369)		
Si	0,026 (0,001)	0,000 (0,000)	1,979 (0,549)	0,059 (0,016)	18,024 (1,148)	2,25 (0,636)	0,003 (0,001)
Mn	0,502 (0,016)	0,015 (0,004)	2,931 (0,235)	0,102 (0,011)	0,851 (0,038)	0,20 (0,02)	0,12 (0,014)
Cr	0,855 (0,020)	0,102 (0,029)	7,481 (1,020)	0,323 (0,059)	0,461 (0,061)	0,38 (0,07)	0,70 (0,16)
V	0,851 (0,037)	0,008 (0,004)	2,681 (0,231)	0,088 (0,010)	0,386 (0,188)	0,10 (0,01)	0,23 (0,11)
O	37,002 (0,188)		25,878 (0,349)	0,776 (0,010)	42,612 (1,091)		

Note: integr. metal = metal composition reintegrated on the basis of the analysed compositions and volume fractions of the blobs and the metal matrix, for details see text. Where distribution coefficients are not listed the respective element in one of the phases is below or very close to the detection limit.

uncertainties in the silicate melt compositions, the values of $D_M^{met/sil}$ also have relatively large errors.

3.1. Attainment of Equilibrium

The homogeneous element concentration profiles in metal and magnesiowüstite of the samples suggest that equilibrium compositions have been attained in most experiments. In particular the broad (~250 μm) diffusion profiles in magnesiowüstite (i.e., Fig. 2c,d) indicate rapid and extensive achievement of chemical equilibrium considering that the initial capsule material consisted of pure MgO. The broad diffusion profiles in magnesiowüstite also indicate equilibrium between the quenched liquid metal and the silicate melt because both phases are usually found in contact (and in equilibrium) with the same magnesiowüstite composition.

Table 4: Magnesiowüstite, metal, and blob compositions (in wt%) determined by electron microprobe analysis and distribution coefficients $D_M^{met/ox}$ of experiments performed with the Si-poor starting material (mix 1, 1a).

# 1554 (1800°C)	magnesiowüstite	metal - matrix			$D^{met/ox}$
Mg	47,083 (0,279)	0,018 (0,006)			
Fe	10,942 (0,139)	81,533 (0,218)			7,45 (0,10)
Ni	0,142 (0,016)	19,591 (0,446)			138,37 (16,09)
Co	0,050 (0,003)	2,020 (0,015)			40,14 (2,04)
Ti	0,985 (0,033)	0,002 (0,001)			
Si	0,108 (0,006)	0,049 (0,009)			0,46 (0,085)
Mn	1,543 (0,027)	0,089 (0,005)			0,057 (0,003)
Cr	2,032 (0,050)	0,211 (0,008)			0,104 (0,005)
V	2,137 (0,062)	0,035 (0,007)			0,016 (0,003)
O	37,347 (0,124)	29,454 (0,114)			

# 1549 (1900°C)	magnesiowüstite	metal - matrix	blob	integr. metal	$D^{met/ox}$
Mg	43,015 (0,379)	0,002 (0,002)	0,008 (0,002)	0,002 (0,002)	
Fe	11,938 (0,122)	83,348 (0,141)	27,570 (2,975)	83,091 (0,154)	6,96 (0,07)
Ni	0,158 (0,008)	19,585 (0,262)	1,306 (0,888)	19,501 (0,265)	123,68 (6,78)
Ti	2,257 (0,096)	0,001 (0,001)	0,152 (0,025)	0,001 (0,001)	
Si	0,276 (0,015)	0,028 (0,002)	9,458 (0,984)	0,072 (0,006)	0,26 (0,03)
Mn	2,394 (0,057)	0,131 (0,014)	15,982 (1,261)	0,204 (0,019)	0,085 (0,01)
Cr	2,622 (0,084)	0,325 (0,015)	6,688 (0,344)	0,355 (0,016)	0,135 (0,01)
V	3,093 (0,074)	0,049 (0,013)	8,117 (0,503)	0,086 (0,015)	0,028 (0,005)
O	36,957 (0,198)	29,459 (0,060)	30,703 (0,259)	0,141 (0,001)	

# 1558 (2000°C)	magnesiowüstite	metal - matrix	blob	integr. metal	$D^{met/ox}$
Mg	47,309 (0,450)	0,027 (0,012)	0,035 (0,004)	0,027 (0,012)	
Fe	9,013 (0,117)	82,507 (0,236)	12,607 (0,316)	82,255 (0,237)	9,13 (0,122)
Ni	0,174 (0,007)	18,518 (0,171)	0,265 (0,065)	18,453 (0,171)	106,29 (4,55)
Co	0,045 (0,002)	1,875 (0,014)	0,054 (0,012)	1,868 (0,014)	41,42 (2,14)
Ti	1,443 (0,043)	0,001 (0,002)	0,350 (0,041)	0,003 (0,002)	
Si	0,139 (0,011)	0,076 (0,013)	17,019 (0,313)	0,136 (0,014)	0,98 (0,105)
Mn	1,748 (0,014)	0,158 (0,007)	23,965 (0,471)	0,244 (0,008)	0,14 (0,004)
Cr	1,874 (0,032)	0,542 (0,014)	3,059 (0,355)	0,551 (0,015)	0,294 (0,009)
V	2,112 (0,036)	0,101 (0,006)	5,541 (0,592)	0,121 (0,008)	0,057 (0,003)
O	37,266 (0,290)	29,648 (0,074)	34,363 (0,132)	0,124 (0,001)	

# 1186 (2200°C)	magnesiowüstite	metal - matrix	blob	integr. metal	$D^{met/ox}$
Mg	48,807 (0,433)	0,002 (0,003)	0,043 (0,017)	0,003 (0,004)	
Fe	9,371 (0,339)	81,748 (0,470)	23,698 (1,614)	81,103 (0,483)	8,66 (0,32)
Ni	0,189 (0,009)	20,367 (0,293)	0,411 (0,221)	20,145 (0,293)	106,50 (5,53)
Ti	1,014 (0,017)	0,001 (0,001)	0,170 (0,108)	0,003 (0,003)	
Si	0,047 (0,002)	0,008 (0,004)	11,020 (0,779)	0,130 (0,013)	2,75 (0,30)
Mn	1,252 (0,017)	0,087 (0,005)	14,370 (0,985)	0,246 (0,016)	0,196 (0,01)
Cr	1,467 (0,058)	0,380 (0,016)	9,734 (0,588)	0,484 (0,022)	0,33 (0,02)
V	1,569 (0,060)	0,039 (0,007)	9,027 (0,750)	0,138 (0,015)	0,09 (0,01)
O	37,367 (0,127)	29,199 (0,114)	35,367	0,393 (0,001)	

# 1551 (2400°C)	magnesiowüstite	metal - matrix	blob	integr. metal	$D^{met/ox}$
Mg	47,620 (0,252)	0,028 (0,006)	0,053 (0,040)	0,029 (0,008)	
Fe	12,233 (0,366)	79,532 (0,399)	66,060 (1,518)	79,060 (0,438)	6,46 (0,20)
Ni	0,204 (0,017)	19,867 (0,208)	0,351 (0,217)	19,184 (0,208)	94,04 (8,39)
Co	0,079 (0,005)	2,195 (0,021)	0,110 (0,026)	2,122 (0,078)	26,86 (1,70)
Ti	0,601 (0,012)	0,002 (0,002)	0,027 (0,029)	0,003 (0,003)	
Si	0,037 (0,002)	0,031 (0,008)	0,277 (0,173)	0,039 (0,013)	1,07 (0,36)
Mn	0,876 (0,017)	0,013 (0,004)	2,621 (0,295)	0,105 (0,015)	0,12 (0,02)
Cr	0,977 (0,033)	0,036 (0,008)	4,464 (0,297)	0,191 (0,018)	0,196 (0,02)
V	0,857 (0,029)	0,003 (0,002)	1,015 (0,381)	0,038 (0,015)	0,045 (0,02)
O	36,472 (0,151)	28,871 (0,075)	22,650 (0,176)	0,793 (0,006)	

Note: inte. metal = reintegrated metal composition on the basis of the analysed compositions and volume fractions of the blobs and the metal matrix, for details see text. Where distribution coefficients are not listed the respective element in one of the phases is below or very close to the detection limit.

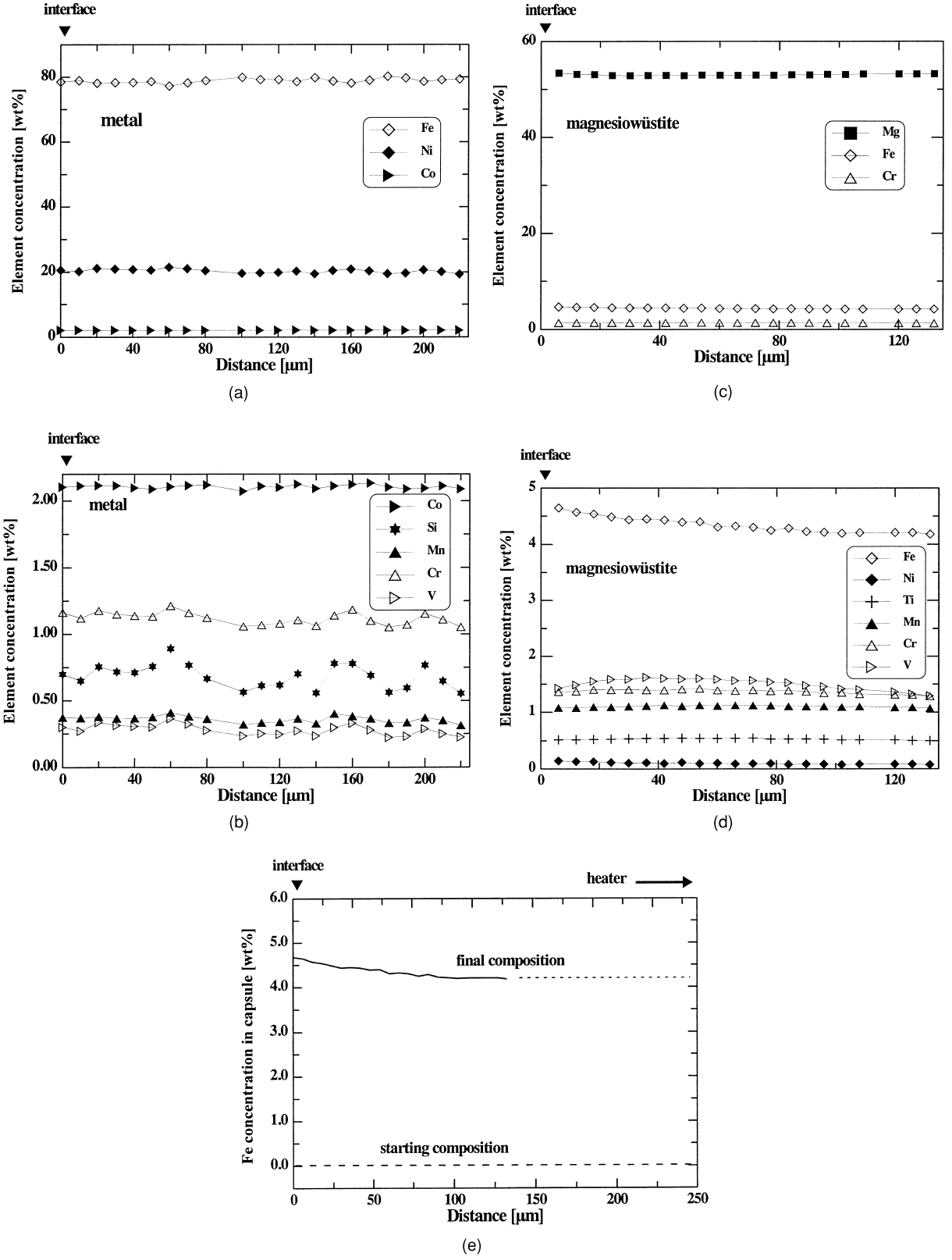

Fig. 2. Element concentration profiles measured in sample 1457. The arrowhead labelled interface marks the contact between the quenched liquid metal and magnesiowüstite (capsule material). (a) Major elements in metal. (b) Trace elements in metal. (c) Major elements in magnesiowüstite. (d) Trace elements in magnesiowüstite. (e) Iron concentration profile from Fig. 2d shown in comparison to the starting Fe-content of the capsule material. The dashed line shows an extrapolation of the data. An arrow indicates the direction of the $LaCrO_3$ heater (for discussion see text).

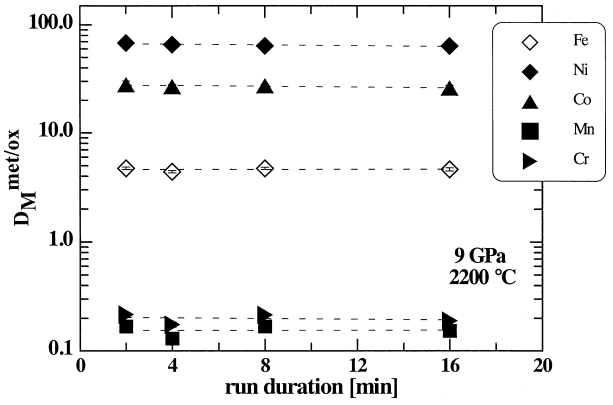

Fig. 3. Metal-magnesiowüstite distribution coefficients as a function of experimental run duration showing that very short run times are sufficient to attain equilibrium compositions in both phases at 2200°C and 9 GPa.

A time-dependent set of experiments was performed with starting material 6a to further assure that equilibrium was attained in the short run times (Table 2). Figure 3 shows the metal-magnesiowüstite distribution coefficients as a function of run duration. No significant variation in the distribution coefficients with time is observed within the uncertainties, indicating that very short run times, e.g., ~ 5 min at 2200°C, are sufficient to attain equilibrium between the metal and magnesiowüstite.

The attainment of equilibrium was further checked by a reversal experiment (#1554, mix 1a) in which the temperature (estimated from power) was first held at 2300° C for 6 min (sufficient to reach equilibrium) before reducing the temperature to a final value of 1800 °C. This lower temperature was maintained for 20 min. The distribution coefficients of this experiment are consistent with the overall trends defined by the other temperature-dependent data (Tables 3 and 4, see Fig. 6b). In comparison to the results of experiment #1245 (1800°C, mix 4a) the distribution coefficients of the T-reversal experiment are slightly lower which may be due to the relatively large uncertainty of temperature in the latter case. In conclusion, the reversal experiment indicates that equilibrium compositions can be approached from compositionally opposite directions.

3.2. Oxygen Fugacity

Experiments were performed at 9 GPa and temperatures in the range 1800–2400 °C with starting materials 1a and 4a (Table 1) in order to vary the amount of silicate liquid present. The oxygen fugacity in these experiments was calculated employing the relation log fO_2 (relative to IW) = 2*log $a_{Fe}^{met}/a_{FeO}^{mw}$ assuming ideal activities of Fe in metal (met) and FeO in magnesiowüstite (mw) (see also Hillgren et al., 1994; Walter and Thibault, 1995; Li and Agee, 1996). Similar calculations have been performed taking the activity coefficients determined at 1 bar for magnesiowüstite by Screcec et al. (1987) and for Fe-Ni alloys by Ramensee and Fraser (1981) into account. The difference in the oxygen fugacities obtained from these two calculations (i.e., ideal activity coefficients and 1 bar activity coefficients) never exceeds 0.6 log bar units (Geßmann et al., 1997).

The log fO_2 values (relative to IW) as a function of temperature, calculated assuming ideal mixing, are shown in Fig. 4. Below a critical temperature the calculated oxygen fugacity is essentially constant while above this temperature it increases significantly. For the experiments using mix 4a (Si/O = 1:1), the critical temperature is ~2200 °C; the calculated oxygen fugacity below 2200 °C is IW-2.7 ±0.03 (log bar units), and above 2200°C the oxygen fugacity increases approximately linearly at 0.4 log bar units per 100 °C (Fig. 4). One anomalous result (# 1418) at 1900°C (Fig. 4) cannot currently be explained; a possible explanation is that the capsule became contaminated by reducing material (e.g., W) during machining. For the experiments using the other starting material (mix 1a, Si/O ~ 1:3), the trend appears similar although it is less well constrained (Fig. 4), and below the critical temperature the calculated log fO_2 values show a relatively large scatter (IW-2.0 ±0.1).

A possible explanation for the increase in fO_2 with temperature above ~2200°C is that oxide material (e.g., the $LaCrO_3$ heater) in the sample assembly becomes reduced at very high temperatures thus releasing oxygen. Further investigations of this possibility are in progress. Overall these results indicate that a particular combination of sample plus capsule material may potentially buffer the experiment within certain P, T, X conditions. At very high temperatures, however, the buffering capacity appears to be limited and overlooking this possibility might result in erroneous conclusions.

The volume proportion of the blobs increases with both increasing temperature and increasing fO_2 (Fig. 5a,b). However, because of the relationship between oxygen fugacity and temperature (Fig. 4), it is not possible to determine the relative importance of these two parameters.

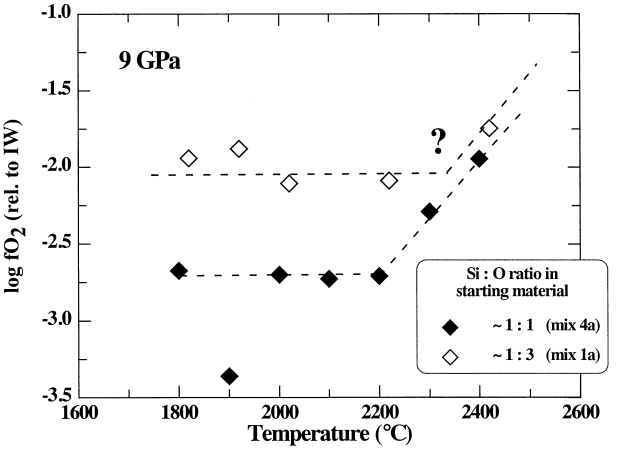

Fig. 4. Calculated log fO_2 values (in log bar units) for the metal-magnesiowüstite assemblages as a function of temperature. The oxygen fugacity appears to be internally buffered below a critical temperature. Above this temperature fO_2 appears to increase rapidly with increasing temperature.

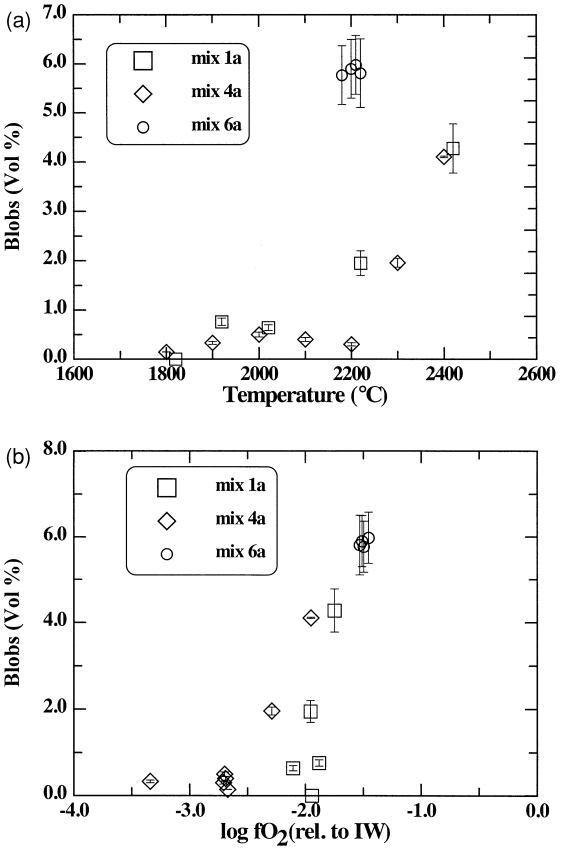

Fig. 5. Volume fraction of the blobs which exsolved from the liquid metal during quenching as a function of temperature (a) and oxygen fugacity (b). The pronounced increase in the proportion of blobs with increasing temperature is also related to an increase in oxygen fugacity.

3.3. Element Partitioning Between Liquid Metal and Magnesiowüstite

The metal-oxide distribution coefficients from two temperature-dependent sets of experiments, using Si-poor and Si-rich starting materials, respectively, are listed in Tables 3 and 4 and shown in Fig. 6. In order to determine the effect of temperature alone, it is necessary to recalculate the results to a constant oxygen fugacity. This can be achieved in two different ways. (a) The metal-oxide distribution coefficients are normalised to the corresponding value for iron, i.e., $D_M^{met/ox}/D_{Fe}^{met/ox}$ if both Fe and element M are divalent or $D_M^{met/ox}/(D_{Fe}^{met/ox})^{3/2}$ for a trivalent element M in exchange with ferrous iron, where M = Co, Ni, Cr, Mn, V. These normalized distribution coefficients are hereafter referred to as two element distribution coefficients $K_DM^{met/ox}$ which are usually considered to be fO_2-independent. (b) The distribution coefficients are recalculated to a certain oxygen fugacity. Both approaches require the valence states of the respective elements in magnesiowüstite to be either known or assumed. The valences of the elements Co, Ni, Mn, Cr, and V have been determined in a companion study (C. K. Geßmann et al., unpubl. data). As expected, Co, Ni, and Mn are divalent while Cr and V are trivalent at 9 GPa in the observed temperature range. The first of the above options is chosen here to facilitate comparison with the results of previous studies.

The $K_DM^{met/ox}$ values for Ni and Co decrease with increasing temperature, with the decrease for Ni being stronger than for Co (Fig. 6a). The distribution coefficients of the elements Mn, Cr, and V progressively increase with temperature (Fig. 6b). The lowest K_D values are obtained for V which also exhibits the weakest increase with increasing temperature while the highest K_D values were determined for Mn which shows the strongest increase with increasing temperature. Chromium displays an intermediate behaviour. Where element concentrations in either of the recovered phases fall distinctly below the calculated detection limits (i.e., the concentrations of Ni and Co in magnesiowüstite at 1800°C (# 1245) or those of V and Mn at 2400°C (# 1551), the respective distribution coefficients are not shown in Figs. 6–10.

Distribution coefficients obtained from the two sets of experiments (Si-rich and Si-poor starting materials) are in good agreement within the errors (although in the case of Ni, the K_DNi values show a large scatter which makes any significant

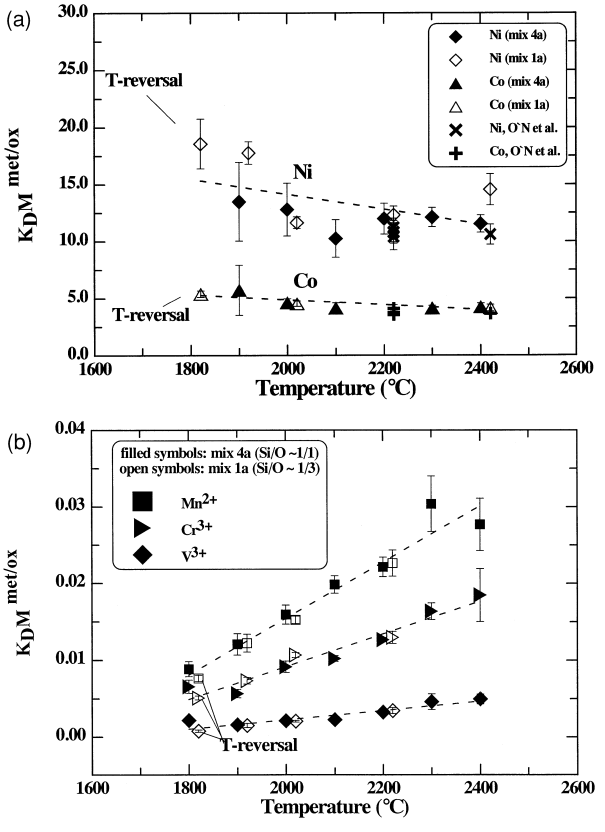

Fig. 6. Metal-oxide distribution coefficients for various elements normalised to $D_{Fe}^{met/ox}$ (i.e., $K_DM^{met/ox} = D_M^{met/ox}/D_{Fe}^{met/ox}$) as a function of temperature at 9 GPa. Open and filled symbols denote results obtained using starting materials with different Si/O ratios; open symbols are displaced from the actual temperature by 20°C for clarity (also in Figs. 6b, 9a,b, and 10). Broken lines show linear regressions to the data for the respective elements. (a) K_DNi and K_DCo versus temperature. Results of O'Neill et al. (1998) at similar P, T conditions are shown for comparison (crosses). (b) K_DMn, K_DCr, and K_DV vs. temperature.

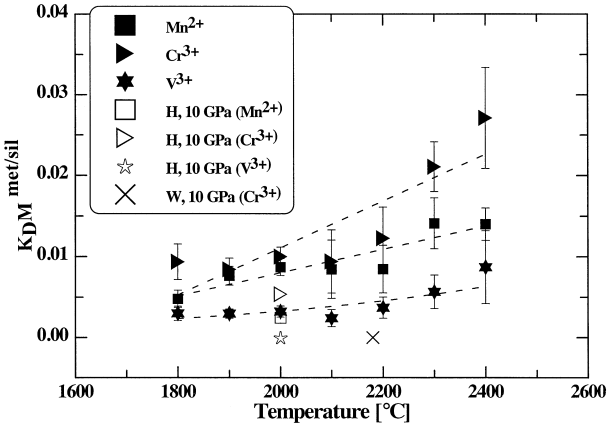

Fig 7. Metal-silicate distribution coefficients for the elements Cr, Mn, and V normalised to D_{Fe} (i.e., $K_DM^{met/sil} = (D_M/D_{Fe})^{met/sil}$) as a function of temperature at 9 GPa. (For comparison, metal-oxide distribution coefficients from the same experiments are shown as filled symbols in Fig. 6b.) $K_D^{met/sil}$ values for Ni and Co are not shown because their element concentrations in the silicate melt are below the detection limits. Note: below 2000°C metal-olivine distribution coefficients are shown whereas at T ≥ 2000°C the symbols show metal - silicate melt distribution coefficients K_DM. The Mn, Cr, and V distribution coefficients determined by Hillgren et al. (1994) and Walker et al. (1993) at 10 GPa are shown for comparison (open symbols and cross, respectively).

differences difficult to recognize; Fig. 6a). The presence of silicate melt of varying proportions and composition, therefore, has no detectable effect on the metal-magnesiowüstite equilibria (Tables 3 and 4, Fig. 6).

3.4. Element Partitioning Between Liquid Metal and Silicate Phases

The presence of silicate melt in experiments in which a Si-rich starting material was used enables metal-silicate distribution coefficients to be calculated and compared with the metal-magnesiowüstite partitioning results. In such experiments, significant amounts of silicate liquid are present (Fig. 1d); although the melt has often migrated significant distances away from the liquid metal, the uniformity of silicate melt and magnesiowüstite analyses enables compositions to be obtained which can be assumed to be in equilibrium with the metal. The normalized metal-silicate distribution coefficients ($K_DM^{met/sil} = D_M/D_{Fe}^{met/sil}$) are very similar to the corresponding metal-oxide values.

The $K_DM^{met/sil}$ values for Mn, Cr, and V increase with increasing temperature as shown in Fig. 7. K_DNi and K_DCo results are not presented because the concentrations of Ni and Co in the quenched silicate melt are very close to or below the detection limits. Metal-silicate partitioning for V, and also for Cr, is very similar to partitioning in the metal-oxide system (cf. Figs. 6b and 7). Both elements show a slight preference for magnesiowüstite in comparison with silicate melt. In the case of Mn, $K_DMn^{met/sil}$ values are distinctly lower than $K_DMn^{met/ox}$ values because Mn partitions into silicate melt in preference to magnesiowüstite.

3.5. Solubilities of Silicon and Oxygen in Liquid Metal

In addition to determining the partitioning behaviour of siderophile elements, the present study also provides information on the solubilities of Si and O in liquid metal (Tables 3 and 4). The O-contents in the liquid metal which have been estimated from the compositions and volume fractions of the blobs have relatively large errors (estimated as ±15%). Figure 8 shows the Si- and O-contents in liquid metal as a function of oxygen fugacity with schematic lines denoting the general trends.

4. DISCUSSION

4.1. Comparison of $K_DM^{met/ox}$ with Literature Data

Comparison of the present results with data from the literature is restricted to Ni, Co, and Cr because, to our knowledge, there are no other systematic high-pressure metal-magnesiowüstite partitioning data for Mn and V. The metal-magnesiowüstite distribution coefficients obtained in this study as a function of temperature are compared in Fig. 9a with the large data set of Urakawa (1991), obtained mainly at 6 and 15 GPa. There are clearly significant differences between the two data sets (Fig. 9a). Our distribution coefficients, obtained at 9 GPa, are significantly lower and suggest a much smaller temperature dependence than the majority of the Urakawa (1991) data. The observed differences cannot be attributed solely to the fact that most of the Urakawa (1991) experiments were performed with sulfur-bearing metal alloys, because his solid (S-free) metal-magnesiowüstite distribution coefficients are not distinctly different from those for S-bearing compositions. The different results cannot be attributed to differences in temperature because the temperature ranges of our study and the Urakawa (1991) data overlap between 1800° and 2200 °C. We suggest that compositional factors are mainly responsible for the observed difference. Our results are obtained

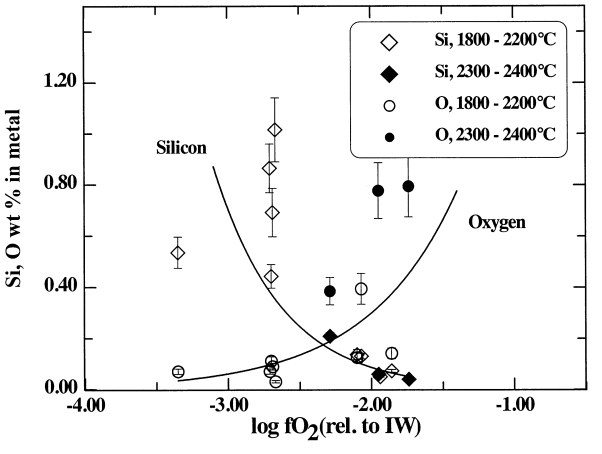

Fig. 8. Silicon and oxygen contents in the liquid metal. Oxygen contents are estimated from the compositions and volume proportions of blobs. The lines denote schematically the general trends observed for the solubility of Si and O in the liquid metal at the investigated temperatures and 9 GPa. (For discussion see text.)

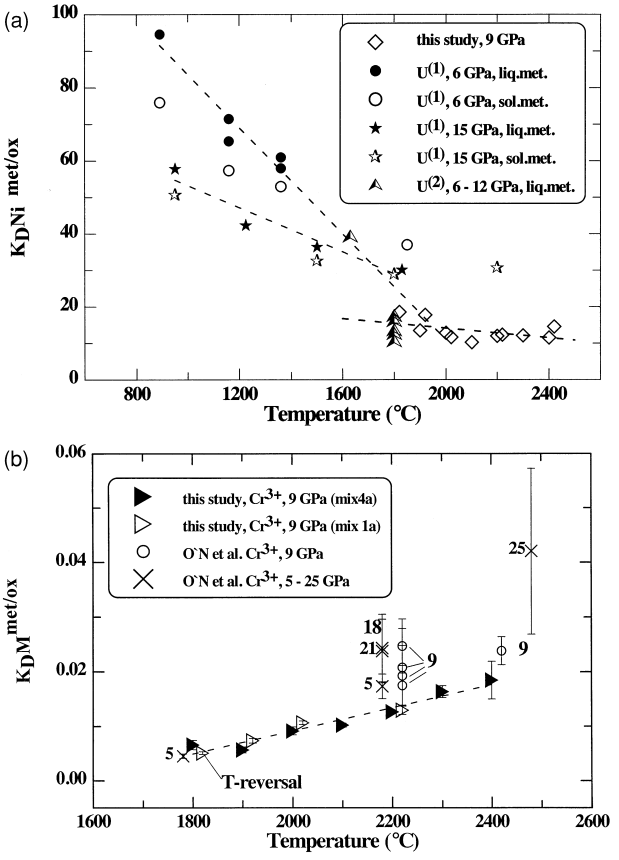

Fig. 9. (a) Comparison of metal-oxide distribution coefficients ($K_D Ni^{met/ox}$) obtained in this study at 9 GPa with the results of Urakawa (1991) at 6–15 GPa, as a function of temperature. $U^{(1)}$ indicates type 1 experiments of Urakawa (1991) in which magnesiowüstite compositions were Fe-rich and $U^{(2)}$ indicates type 2 experiments of Urakawa (1991) in which magnesiowüstite compositions were MgO-rich. Regression lines for the Urakawa (1991) experiments are only shown for distribution coefficients obtained with liquid metal. The large deviations between the results of the two studies appear to be due to differences in magnesiowüstite composition, as discussed in the text. (b) Comparison of the temperature dependent $K_D Cr$ data obtained in this study at 9 GPa with the data of O'Neill et al. (1998) obtained in the same temperature range at 5–25 GPa (numbers adjacent to the symbols indicate pressure in GPa).

from experiments with MgO-rich magnesiowüstite compositions (X_{FeO} = 0.01–0.14), while most of the Urakawa (1991) experiments were performed with FeO-rich magnesiowüstite ("type 1" experiments with X_{FeO}= 0.78–0.98). Some of the Urakawa (1991) partitioning data, however, are for FeO-poor magnesiowüstite ("type 2" experiments with X_{FeO} = 0.10–0.19), and these are also shown in Fig. 9a. Except for one datum (1600°C, 7 GPa) for magnesiowüstite with an intermediate Fe-content (X_{FeO}= 0.29), the results of the "type 2" experiments (1800°C, 6, 7, and 12 GPa) fall exactly on the trend defined by our results (even though the Urakawa (1991) compositions were S-bearing). Thus we conclude that the magnesiowüstite composition, i.e., nonideal mixing behaviour in magnesiowüstite at high pressure and temperature, strongly effects the partitioning behaviour of Ni. Specifically, the distribution coefficients for Ni between Fe-rich magnesiowüstite and metal are distinctly higher compared to the values for Fe-poor magnesiowüstite and metal. A detailed analysis of these results and a discussion of the nonideal mixing behaviour of Ni in magnesiowüstite will be presented elsewhere (C. K. Geßmann and D. C. Rubie, unpubl. data).

Our results show that the normalized distribution coefficients $K_D Ni$ and $K_D Co$ decrease slightly with increasing temperature. The K_D-values for Ni and Co obtained by O'Neill et al. (1998) at 9 GPa are compared with our results in Fig. 6a and agree within error. However, because our data have been obtained over a relatively large temperature interval, they define the temperature dependence (at constant pressure) better than the data of O'Neill et al. (1998); Fig. 6a.

The $K_D Cr$ values of our study are compared to those of O'Neill et al. (1998) in Fig. 9b which shows systematic deviations between the two data sets. The distribution coefficients reported by O'Neill et al. (1998) are larger than our values at all pressures, including 9 GPa. We are currently unable to fully explain this discrepancy. The systematic differences might be due to systematic differences in the determined volume fractions of exsolved blobs in the two studies. i.e., whenever a large volume fraction is present, the distribution coefficients for major blob-forming elements, such as Mn and Cr, have relatively large errors. The volume fractions of blobs in the samples of O'Neill et al. (1998) are large compared to those in most of our samples.

4.2. Comparison of Metal-Silicate Distribution Coefficients

Hillgren et al. (1994) compared their metal-silicate distribution coefficients for Fe, Ni, Co, W, Mo, Mn, Cr, and V obtained at 10 GPa, 2000 °C and fO_2 = −1.6 (rel. to IW) with data obtained at 1 bar and 1260 °C by Jones and Drake (1986) and Drake et al. (1989). Because the effects of temperature and pressure cannot be separated when making this comparison, we cannot directly compare the temperature-dependence of our data with their results. A similar problem arises when comparing our $K_D Cr^{met/sil}$ values with the results of Walker et al. (1993). However, the results of these two earlier studies obtained at 10 GPa are compared with our K_D values (9 GPa) in Fig. 7. The D_{Fe} normalized distribution coefficients of Walker et al. (1993) are distinctly lower, and those of Hillgren et al. (1994) are slightly lower compared to our data. In contrast to our experiments, Al_2O_3 is present in the silicate liquid in the studies of Walker et al (1993) and Hillgren et al. (1994) which according to the results of Walter and Thibault (1996) and Hillgren et al. (1996) should increase the metal-silicate partitioning coefficients of siderophile elements due to a higher degree of polymerization of the silicate melt structure. The distinctly lower $K_D Cr^{met/sil}$ value of Walker et al. (1993) compared to our results may, therefore, be due to the presence of sulphur in their experiments.

For Ni and Co there are significant discrepancies in the determined effects of temperature on metal-silicate partitioning between different studies. Thibault and Walter (1995) found that $K_D Co$ decreases with increasing temperature while temperature has a negligible effect on Ni-partitioning. On the other

hand, Agee et al. (1995) reported that K_DNi increases significantly with temperature at constant pressure. Unfortunately our data cannot be used to resolve these discrepancies because the Ni and Co concentrations in the silicate liquid are below detection limits.

4.3. Depletion of Manganese, Chromium, and Vanadium in the Earth's Mantle

Ringwood (1966) noted that the elements Mn, Cr, and V are depleted relative to C1 chondrites in the Earth's mantle. Since then there has been considerable discussion regarding the origin of this depletion. Possible explanations include volatility and/or the incorporation of these elements in the Earth's core (e.g., Ringwood, 1966; Dreibus and Wänke, 1979; Drake et al., 1989, O'Neill, 1991). Experimental data suggest that these elements become increasing siderophile with increasing temperature at 1 bar (e.g., Rammensee et al. 1983, Drake et al., 1989) and at high pressure (Ringwood et al., 1990). Our current results also show that Mn, Cr, and V progressively partition into the metallic phase (i.e., become increasingly siderophile) with increasing temperature at 9 GPa, thus providing further evidence that core-mantle fractionation contributed to their depletion in the Earth's mantle.

4.4. Extrapolation to Higher Temperatures

It has been suggested that element partitioning during core separation at very high temperatures may be sufficient to explain (at least partly) the current abundances of siderophile elements in the mantle (e.g., Murthy, 1991, 1992; Walker et al., 1993). An extrapolation of our data to higher temperatures is shown in Fig. 10. The metal-oxide distribution coefficients of the moderately siderophile elements Mn, Cr, and V exhibit a stronger temperature dependence than those of Ni and Co. By extrapolation to higher temperatures (e.g., ~3200°C) the Mn, Cr, and V distribution coefficients attain values close to those required to explain the current mantle abundances by equilibrium core-mantle separation. In contrast, the extrapolated distribution coefficients of Ni and Co do not reach the required values and do not converge to identical values (as required by an equilibrium model of core formation). However, in addition to the effects of temperature, other variables, in particular pressure, have been shown to significantly influence the partitioning behaviour of siderophile elements in metal-silicate and metal-oxide systems. The distribution coefficients for Ni and Co decrease strongly and become approximately identical at pressures above 30 GPa, as shown for example by Thibault and Walter (1995) and Li and Agee (1996) for metal-silicate partitioning and by Geßmann et al. (1995) and O'Neill et al. (1998) for the metal-magnesiowüstite system. Consequently, the combined effects of pressure and temperature on siderophile element partitioning must be considered carefully before an equilibrium model for core formation can be excluded. The effects of pressure on the metal-oxide partitioning of Mn, Cr, and V will be discussed separately (Geßmann and Rubie, unpubl. data).

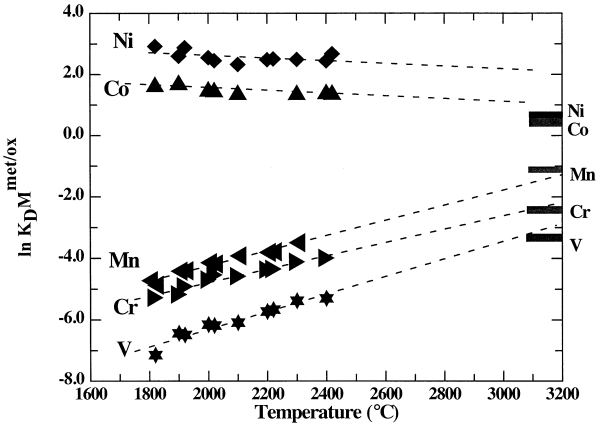

Fig. 10. Extrapolation of the experimentally-determined metal-magnesiowüstite distribution coefficients (K_DM) to higher temperatures in comparison with the values required to explain current mantle abundances by equilibrium core formation. The latter values (indicated at the right hand side of the diagram) are estimated from the compilation of McDonough and Sun (1995, Table 6) assuming 15% light element(s) in the core.

4.5. Silicon and Oxygen As Possible Light Constituents in the Earth's Core

Figure 8 shows that very reducing conditions are required to dissolve relatively large amounts of Si in liquid metal at 9 GPa. For oxygen the opposite applies, and the highest solubilities of O are observed when the oxygen fugacity is high. Over the range of conditions of this study, the solubilities of both Si and O never exceed 1 wt% and are thus far below the estimated 10–15 wt% of light constituent(s) in the core (e.g., Poirier, 1994). In addition, the range of conditions under which the amounts of dissolved Si and O are balanced in a 1:2 ratio in liquid metal are extremely limited (Fig. 8) thus indicating the difficulty of dissolving an SiO_2 component in liquid metal (see also O'Neill et al., 1998). Based on these results, neither Si, O, nor a combination of these elements appear to be viable candidates for the main light components in the core.

Acknowledgments—We thank Hubert Schulze and Oskar Leitner for very careful sample preparation and Detlef Krauße for assistance with microprobe analyses. We would like to thank Dr. F. Wallrafen who kindly provided access to an image analysis system at the University of Bonn where part of the image analysis was performed. We gratefully acknowledge discussions with Hugh O'Neill, Sumit Chakraborty and colleagues from the Deutsche Forschungs Gemeinschaft (DFG) priority program on 'Element Partitioning'. The careful reviews by F. Guyot, K. Righter, and an anonymous reviewer are greatly appreciated. This study was funded by DFG grant RU 437/3-2 and by the EC 'Human Capital and Mobility—Access to Large Scale Facilities' programme (contract No. ERBCHGECT940053 to D. C. Rubie).

REFERENCES

Agee C. B., Li J., Shannon M. C., and Circone S. (1995) Pressure-temperature phase diagram for the Allende meteorite. *J. Geophys. Res.* **100**, 17725–17740.

Benz W., Slattery W. S., and Cameron A. G. W. (1986) The origin of the moon and the single impact hypothesis. *Icarus* **66**, 515–535.

Brümmer O. (1977) *Mikroanalyse mit Elektronen und Ionensonden*. VEB Deutscher Verlag für Grundstoffindustrie.

Canil D. (1991) Experimental evidence for the exsolution of cratonic peridotite from a high-temperature harzburgite. *Earth Planet. Sci. Lett.* **106**, 64.

Drake M. J., Newsom C. J., and Capobianco C. J. (1989) Vanadium, chromium, and manganese in the Earth, Moon, EPB, and SPB and the origin of the Moon: Experimental studies. *Geochim. Cosmochim. Acta* **53**, 2101.

Drake M. J., McFarlane E. A., Gasparik T., and Rubie D. C. (1993) Mg-perovskite/silicate melt and majorite garnet/silicate melt partition coefficients in the system CaO-MgO-SiO_2 at high temperatures and pressures. *J. Geophys. Res.* **98**, 5427–5431.

Dreibus G. and Wänke H. (1979) On the chemical composition of the moon and the eucrite parent body and comparison with composition of the Earth: The case of manganese, chromium, and vanadium. *Lunar Planet. Sci.* **10,** 315–317.

Geßmann C. K., Rubie D. C., and O'Neill H. St. C. (1995) Partitioning of siderophile elements between liquid metal, silicate melt and magnesiowüstite: Dependence of pressure, T, fO_2, and implications for the formation of the Earth's core. Suppl. *EOS Trans. Amer. Geophys. Union* **76**, F553.

Geßmann C. K., McCammon C., and Rubie D. C. (1997) Oxygen fugacity constraints in unbuffered multianvil high pressure experiments. *Terra Nova* **9**, *Abstract Suppl*. **1**, *EUG* **9**, 434.

Hillgren V. J. (1991) Partitioning behavior of nickel, cobalt, molybdenum, and tungsten between basaltic liquid and Ni-rich metal: Implications for the origin of the Moon and lunar core formation. *Geophys. Res. Lett*. **18**, 2077–2080.

Hillgren V. J., Drake M. J., and Rubie D. C. (1994) High pressure and high temperature experiments on core-mantle segregation in the accreting Earth. *Science* **264**, 1442–1445.

Hillgren V. J, Drake M. J., and Rubie D. C. (1996) High pressure and high temperature metal-silicate partitioning of siderophile elements: The importance of silicate liquid composition. *Geochim. Cosmochim. Acta* **60**, 2257–2263.

Holzheid A., Borisov A., and Palme H. (1994) The effect of oxygen fugacity and temperature on solubilities of nickel, cobalt, and molybdenum in silicate melts. *Geochim. Cosmochim. Acta* **58**, 1975–1981.

Ito E., Takahashi E., and Matsui Y. (1984) The mineralogy and chemistry of the lower mantle: An implication of the ultrahigh-pressure phase relations in the system MgO-FeO-SiO_2. *Earth Planet. Sci. Lett.* **67**, 238–248.

Ito E., Morooka K., Ujike O., and Katsura T. (1995) Reactions between molten iron and silicate melts at high pressure: Implications for the chemical evolution of Earth's core. *J. Geophys. Res.* **100**, 5901–5910.

Jones J. H. and Drake M. J. (1986) Geochemical constraints on core formation in the Earth. *Nature* **322**, 221–228.

Kato T., Ringwood A. E., and Irifune T. (1988a) Experimental determination of element partitioning between silicate perovskites, garnets, and liquids: Constraints on early differentiation of the mantle. *Earth Planet. Sci. Lett.* **89**, 123–145.

Kato T., Ringwood A. E., and Irifune T. (1988b) Constraints on element partition coefficients between $MgSiO_3$ perovskite and liquid determined by direct measurements. *Earth Planet. Sci. Lett.* **90**, 65–68.

Keppler H. and Rubie D. C. (1993) Pressure induced coordination changes of transition-metal ions in silicate melts. *Nature* **364**, 221–228.

Kesson S. E. and Fitz Gerald J. D. (1992) Partitioning of MgO, FeO, NiO, MnO and Cr_2O_3 between magnesian silicate perovskite and magnesiowüstite: Implications for the origin of inclusions in diamond and the composition of the lower mantle. *Earth Planet. Sci. Lett.* **111**, 229–240.

Li J. and Agee C. B. (1996) Geochemistry of mantle-core formation at high pressure. *Nature* **381**, 686–689.

Liebermann R. C. and Wang W. (1992) Characterization of sample environment in a uniaxial split-sphere apparatus. In *High Pressure Research: Application to Earth and Planetary Sciences* (ed. Y. Syono and M. H. Manghnani), pp. 19–31. Terrapub.

Malavergne V., Guyot F., Wang Y., and Martinez I. (1997) Partitioning of nickel, cobalt, and manganese between silicate perovskite and periclase: A test of crystal field theory at high pressure. *Earth Planet. Sci. Lett.* **146**, 499–509.

McDonough W. F. and Sun S.-S. (1995) The composition of the Earth. *Chem. Geol.* **120**, 223–253.

McFarlane E. A., Drake J. M., and Rubie D. C. (1994) Element partitioning between Mg-perovskite, magnesiowüstite, and silicate melt at conditions of the Earth's mantle. *Geochim. Cosmochim. Acta* **58**, 5161–5172.

Murthy V. R. (1991) Early differentiation of the Earth and the problem of mantle siderophile elements: A new approach. *Science* **253**, 303–306.

Murthy V. R. (1992) Geochemical evidence for an initially molten Earth. *Phys. Earth Planet. Intl.* **71**, 46–51.

O'Neill H. St. C. (1991) The origin of the moon and the early history of the Earth—A chemical model. Part 2: The Earth. *Geochim. Cosmochim. Acta* **55**, 1159–1172.

O'Neill H. St. C., Canil C., and Rubie D. C. (1998) Metal-oxide equilibria to 2500°C and 25 GPa: Implications for core formation and the light component in the Earthś core. *J. Geophys. Res.* (in press).

Ohtani E. and Ringwood A. E. (1984) Composition of the core, I. Solubility of oxygen in molten iron at high temperatures. *Earth Planet. Sci. Lett.* **71**, 85–93.

Ohtani E., Yurimoto H., Segawa T., and Kato T. (1995) Element partitioning between $MgSiO_3$ perovskite, magma, and molten iron: Constraints on the earliest processes of the Earth-Moon system. In *The Earth's Central Part: Its Structure and Dynamics*. (ed. T. Yukutake), pp. 287–300. Terra. Sci. Publ.

Ohtani E., Yurimoto H., and Seto S. (1997) Element partitioning between metallic liquid, silicate liquid, and lower-mantle minerals: Implications for core formation of the Earth. *Phys. Earth Planet. Interiors* **100**, 97–114.

Poirier J.-P. (1994) Light elements in the Earth's outer core: A critical review. *Phys. Earth Planet. Interiors* **85**, 319–337.

Rammensee W. and Fraser D. G. (1981) Activities in solid and liquid Fe-Ni and Fe-Co alloys determined by Knudsen cell mass spectrometry. *Ber. Bunsenges. Phys. Chem.* **85**, 588–592.

Rammensee W., Palme H., and Wänke H. (1983) Experimental investigation of metal-silicate partitioning of some lithophile elements (tantalum, manganese, vanadium, and chromium). *Lunar Planet. Sci.* **14**, 628–629.

Ramsden A. R. and French D. H. (1990) Routine trace-element capabilities of electron-microprobe analysis in mineralogical investigations: An empirical evaluation of performance using spectrochemical standard glasses. *Canadian Mineral.* **28**, 171–180.

Righter K., Drake M. J., and Yaxley G. (1997) Prediction of siderophile element metal/silicate partition coefficients to 20 GPa and 2800 °C: The effects of pressure, temperature, oxygen fugacity, and silicate and metallic melt compositions. *Phys. Earth Planet. Interiors* **100**, 115–134.

Ringwood A. E. (1966) The chemical composition and origin of the Earth. In *Advances in Earth Sciences* (ed. P. M. Hurley), pp. 287–356. MIT Press.

Ringwood A. E., Kato T., Hibberson W., and Ware N. (1990) High pressure geochemistry of chromium, vanadium, and manganese and implications for the origin of the Moon. *Nature* **347**, 174–176.

Rubie D. C., Karato S., Yan H., and O'Neill H. St. C. (1993a) Low differential stress and controlled chemical environment in multianvil high-pressure experiments. *Phys. Chem. Minerals* **20**, 315–322.

Rubie D. C., Ross II C. R., Carroll M. R., and Elphick S. C. (1993b) Oxygen self-diffusion in $Na_2Si_4O_9$ liquid up to 10 GPa and estimation of high-pressure melt viscosities. *Amer. Mineral.* **78**, 574.

Screcec I., Ender A., Woermann E., Gans W., Jacobsson E., Erikson G., and Rosen E. (1987) Activity-Composition relations of the mag-

nesiowüstite solid solution series in equilibrium with metallic iron in the temperature range 1050–1400 K. *Phys. Chem. Minerals* **14**, 492–498.

Stevenson D. J. (1990) Fluid dynamics of core formation. In *Origin of the Earth* (ed. H. E. Newsom and J. H. Jones), pp. 231– 249. Oxford Univ. Press.

Thibault Y. and Walter M. J. (1995) The influence of pressure and temperature on the metal-silicate partition coefficients of nickel and cobalt in a model C1 chondrite and implications for metal segregation in a deep magma ocean. *Geochim. Cosmochim. Acta* **59**, 991–1002.

Trønnes R. G., Canil D., and Wei K. (1992) Element partitioning between silicate minerals and coexisting melts at pressures of 1–27 GPa and implications for mantle evolution. *Earth Planet. Sci. Lett.* **111**, 241–255.

Underwood E. E. (1970) *Quantitative Stereology*. Addison-Wesley Publ. Co., Inc.

Urakawa S. (1991) Partitioning of nickel between magnesiowüstite and metal at high pressure: Implications for core-mantle equilibrium. *Earth Planet. Sci. Lett.* **105**, 293–313.

Walker D., Norby L., and Jones J. H. (1993) Superheating effects on metal-silicate partitioning of siderophile elements. *Science* **262**, 1858–1861.

Walter M. J. and Thibault Y. (1996) Partitioning of tungsten and molybdenum between metallic liquid and silicate melt. *Science* **270**, 1186–1189.